

Hybrid deep learning and active contour for segmenting hazy images

Firhan Azri Ahmad Khairul Anuar¹, Jenevy Jone², Raja Farhatul Aiesya Raja Azhar³,
Abdul Kadir Jumaat^{1,4}

¹Faculty of Computer and Mathematical Sciences, Universiti Teknologi MARA, Shah Alam, Malaysia

²Finance Risk Cost Control, Shangri-La Rasa Ria, Pantai Dalit Tuaran, Kota Kinabalu, Malaysia

³Faculty of Computing and Informatics, Universiti Malaysia Sabah, Kota Kinabalu, Malaysia

⁴Institute for Big Data Analytics and Artificial Intelligence (IBDAAI), Universiti Teknologi MARA, Shah Alam, Malaysia

Article Info

Article history:

Received Mar 26, 2025

Revised Jun 30, 2025

Accepted Jul 10, 2025

Keywords:

Active contour

Deep learning

Hazy image

Image segmentation

Variational level set

ABSTRACT

Image segmentation seeks to distinguish the foreground from the background for further analysis. A recent study presented a new active contour model (ACM) for image segmentation, termed Gaussian regularization selective segmentation (GRSS). This interactive ACM is effective for segmenting certain objects in images. However, a weakness of the GRSS model becomes apparent when utilized on hazy images, as it is not intended for such conditions and produces inadequate outcomes. This paper introduces a new ACM for segmenting hazy images that hybridizes a pretrained deep learning model, namely DehazeNet, with the GRSS model. Specifically, the haze-free images are estimated using DehazeNet, which fuses the information with the GRSS model. The new formulation, designated as GRSS with DehazeNet (GDN), is addressed via the calculus of variations and executed in MATLAB software. The segmentation accuracy was evaluated by calculating Error, Jaccard, and Dice metrics, while efficiency was determined by measuring processing time. Despite the increased processing time, numerical experiments demonstrated that the GDN model achieved higher accuracy, as indicated by the lower error and higher Jaccard and Dice than the GRSS model. The GDN model can potentially be formulated in the vector-valued image domain in the future.

This is an open access article under the [CC BY-SA](https://creativecommons.org/licenses/by-sa/4.0/) license.



Corresponding Author:

Abdul Kadir Jumaat

Faculty of Computer and Mathematical Sciences, Institute for Big Data Analytics and Artificial Intelligence (IBDAAI), Universiti Teknologi MARA

Kompleks Al-Khawarizmi, 40450 Shah Alam, Selangor, Malaysia

Email: abdulkadir@tmsk.uitm.edu.my

1. INTRODUCTION

Digital image processing involves interpreting and applying digital images to extract information, enhancing clarity and practicality for observation. Notably, numerous techniques exist within the realm of image processing, including image dehazing and image segmentation. In particular, image segmentation involves partitioning or delineation of an image into distinct objects or regions for subsequent processing. This technique finds applications in areas such as medical image analysis [1]–[5], robotics, pattern recognition, image understanding, and computer vision [6]–[8]. An established method for image segmentation is the active contour model (ACM), which relies on mathematical modeling. Furthermore, ACMs demonstrate significant efficacy in producing high-quality image segmentation and excel in the

extraction of similar regions [9]. The ACMs present in various applications [10]–[12] can be categorized into global and interactive segmentation.

Global segmentation aims to segment an image object over a whole image. In [7], a local and global ACM hybrid was formulated in a fuzzy theoretical framework to segment images with intensity inhomogeneity. Moreover, to segment medical images, [13] and [14] successfully developed a hybrid ACM and a simultaneous segmentation and correction model, respectively. Another popular strategy to achieve successful image segmentation is utilizing the saliency map of images as conducted by [15], [16]. However, all the models may produce unsatisfactory results if the targeted object approximates the neighboring object or image noise. Hence, to address this issue, an alternative way is to use interactive image segmentation techniques.

Interactive segmentation is a technique for segmenting an image that focuses on the selected object or region of it [17]. In the image processing community, interactive image segmentation is also known as selective image segmentation. In addition to robotics, applications suitable for the incorporation of interactive segmentation techniques include research fields such as medical imaging [18]–[20], as well as pattern recognition [21]. The models require the end user to be interactively involved in determining the targeted object by defining a set of markers around it. Accordingly, the models will utilize the marker set to achieve an accurate result. One of the earliest interactive segmentation models was developed in [22], which utilized a distance function coupled with the regularization (total variation) term. However, the model may produce poor results when the object boundary is weak. Thus, a one-level-set idea with area constraint was proposed by [23] to overcome the limitation. Although the model is successful, it requires substantial computing costs. Therefore, to enhance efficiency, the model in [24] was proposed. The model is effective for the small and moderate size of an image. To segment large size of images, Jumaat and Chen [25] successfully proposed a new interactive ACM.

Recently, Saibin and Jumaat [12] have successfully developed an interactive ACM, namely Gaussian regularization selective segmentation (GRSS), since the previous models mentioned above are less efficient with regard to segmenting images having intensity inhomogeneities. However, GRSS is not equipped to segment images affected by haze, leading to suboptimal segmentation outcomes. Note that haze in images is unavoidable, particularly during the acquisition phase for real images. According to Ali *et al.* [26], it can be challenging to segment a real image with the presence of haze. Haze is interpreted as an atmospheric phenomenon caused by particles such as dust, smoke, and other dry particles suspended in the air, affecting obscure visibility and sky clarity. This demonstrates the significance of the image dehazing process for real images.

The commonly used haze reduction techniques, such as DehazeNet [27], can enhance the image quality. As a deep learning-based method, DehazeNet is powerful in reducing image haze. Hence, this study presents a new ACM for segmenting hazy images that hybridizes the pretrained DehazeNet with the GRSS model. Specifically, we estimate the haze-free images using DehazeNet and fuse the information with the GRSS model. The newly developed formulation is designated as the GRSS with DehazeNet (GDN) model. The subsequent parts of this document are systematically structured into three distinct sections. Section 2 describes the methodology employed in the study. Meanwhile, Section 3 addresses the results and discussion, whereas Section 4 will cover the conclusion and recommendations.

2. METHOD

Section 2 discusses the research methodology for the proposed model. Additionally, the implementation process was presented to allow a precise comprehension with regard to how image dehazing and segmentation work. Figure 1 illustrates the methodology phase flow involved in this research.

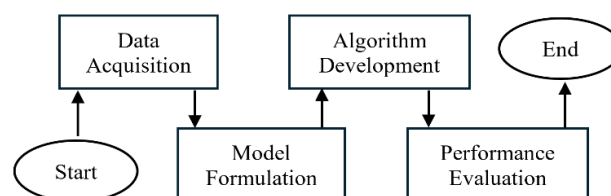


Figure 1. Flow of the research methodology

There are four phases included in this research, as illustrated in Figure 1. The first phase is data acquisition from available databases. Next, the formulation of the GDN model will be discussed. All the steps

to solve the proposed model are explained in detail in this phase as well. Subsequently, a MATLAB algorithm will be developed to implement the model. Finally, the proposed model's image segmentation results will be compared to the existing model. The subsequent subsection provides a thorough explanation of each phase.

2.1. Data acquisition

The first phase of this study is to acquire real test images from publicly available databases [28]–[32]. In addition, the benchmark images, which are essential for comparing and evaluating different models in this study, were also retrieved from the same sources. The images are resized to a size of 256×256 pixels using MATLAB R2023a software.

2.2. Model formulation

In this study, the GRSS model, which was recently proposed by [12], is considered. In the model, a set of markers, also known as geometrical constraint A , is utilized, located near the targeted object. The distance energy term $DF = \int_D P_d H(\phi) dD$, which is formulated in level set function $\phi(x, y)$, in image domain D is used where the Euclidean distance, P_d of each pixels in D from A is applied as defined in [12]. Then, the GRSS model is mathematically defined as in (1).

$$\min \left\{ GRSS = \frac{1}{2} \int_D (z_0 - (f_1 H(\phi) + f_2 (1 - H(\phi))))^2 dD + \theta \int_D P_d H(\phi) dD \right\} \quad (1)$$

The Heaviside function is denoted by $H(\phi)$, the constant θ is the coefficient for distance term, the intensity average inside segmentation contour is denoted by $f_1(x, y) = k_\sigma * [H(\phi)z_0]/k_\sigma * H(\phi)$, and $f_2(x, y) = k_\sigma * [1 - H(\phi)z_0]/k_\sigma * [1 - H(\phi)]$ indicates the intensity average outside the contour such that $k_\sigma = e^{-(x^2+y^2)/2\sigma^2}$. The GRSS model is capable of effectively segmenting an object in an intensity inhomogeneity image. The segmented contour resulting from the segmentation process using the GRSS model can be adjusted interactively by defining a suitable location of the marker set A . However, the GRSS model is less effective in segmenting images with haze. Dust, smoke, and other dry airborne particles will cause digital images to be corrupted during the image capture process, making it challenging to segment using an image segmentation model. To reduce image haze, image dehazing techniques such as DehazeNet [27] are frequently used. In DehazeNet, the input image with haze, Z_0 , can be estimated using the atmospheric scattering function (2).

$$Z_0(x, y) = J(x, y)T(x, y) + A(1 - T(x, y)), \quad (2)$$

Here, $Z_0(x, y)$ refers to an observed intensity (input image with haze), $J(x, y)$ represents a scene radiance (dehazed image), $A(x, y)$ is the atmospheric light, and $T(x, y)$ resembles the transmission map describing the light that reaches the camera. Note that the DehazeNet was developed utilizing a convolutional neural network idea where the input is Z_0 while the output is $T(x, y)$. The training dataset consists of 100,000 synthetic patches where the activation function applied is the bilateral rectified linear unit (BReLU). The loss function applied is mean squared error with Stochastic gradient descent as the optimizer. Considering the atmospheric light, the dehazing algorithm estimates the transmission map, and to obtain the scene radiance (dehazed image) J , (2) is rewritten as (3).

$$J(x, y) = (I(x, y) - A(1 - T(x, y)))/T(x, y). \quad (3)$$

With all the ingredients, a new interactive ACM to effectively segment images with haze can be formulated by reformulating the recent GRSS model in (1) by integrating the output from the pretrained DehazeNet method proposed by [27]. The new formulation is named the GDN model in (4).

$$\min \left\{ \begin{array}{l} GDN = \frac{\alpha_1}{2} \int_D (J - (g_1 H + g_2 (1 - H)))^2 dD + \\ \theta \int_D P_d H dD + \frac{\alpha_2}{2} \int Z_0 - (h_1 H + h_2 (1 - H))^2 dD \end{array} \right\}, \quad (4)$$

Here, Z_0 denotes an input hazy image, J indicates the output of DehazeNet, and α_1 demonstrates the coefficient for the fitting term based on the output image from DehazeNet, α_2 is the coefficient for the fitting term based on the original hazy input image. The terms $h_1(x, y) = k_\sigma * [H(\phi)Z_0]/k_\sigma * H(\phi)$ and $g_1(x, y) = k_\sigma * [H(\phi)J]/k_\sigma * H(\phi)$ are the average image intensities inside the segmentation contour of Z_0 and J , respectively. The terms $h_2(x, y) = k_\sigma * [1 - H(\phi)Z_0]/k_\sigma * [1 - H(\phi)]$ and $g_2(x, y) = k_\sigma *$

$[1 - H(\phi)]/k_\sigma * [1 - H(\phi)]$ indicate the average of image intensities outside the segmentation contour of Z_0 and J , respectively.

By calculus of variations, (5) is derived in order to solve the GDN.

$$\delta(\phi)\{\alpha_1[J - g_1H(\phi) - g_2(1 - H(\phi))](g_1 - g_2) + \alpha_2[Z_0 - h_1H(\phi) - h_2(1 - H(\phi))](h_1 - h_2) - \theta P_d\}. \quad (5)$$

Here, the gradient descent method can be used to solve (5) to obtain (6).

$$\frac{\partial \phi}{\partial t} = \delta(\phi)\{\alpha_1[J - g_1H(\phi) - g_2(1 - H(\phi))](g_1 - g_2) + [Z_0 - h_1H(\phi) - h_2(1 - H(\phi))](h_1 - h_2) - \theta P_d\}. \quad (6)$$

In other words, the model GDN in (4) is minimized by solving (6).

2.3. Algorithm development

This phase discusses the implementation regarding the suggested model in the segmentation process. There are two stopping criteria utilized to stop the process automatically. Firstly, the tolerance value, $tol = 1 \times 10^{-6}$, and secondly, the maximum number of iterations, $maxit=100$. Equation (6) was implemented using MATLAB R2023a software. The MATLAB Algorithm 1 provided summarizes the steps involved in the GDN model implementation process.

Algorithm 1. Algorithm to implement the GDN model

1. Evaluate J using DehazeNet of Equation (3).
`>> HazeImage=input image; >> J=DehazeNet(HazeImage);`
2. Set the value tol , $maxit$, θ , σ , α_1 , and α_2 .
`>>tol=1e-6; maxiter=100; theta=80; sigma =12; alpha1=5, alpha2=1;`
3. Define the marker set A .
`>>mx=[59;115;66;7]; >>my=[11;99;192;99];`
4. Initialize the level set function ϕ .
`>>phi=double(bwdist(poly2mask(mx,my)));`
5. **For** $iteration=1$ to $maxit$ or $\frac{\|\phi^{k+1}-\phi^k\|}{\|\phi^k\|} \leq tol$ **do**
 Evolve the level set function ϕ based on (6).
 Regularize ϕ by convolving with k_σ .
end for
`>> for iteration=1: maxit`
`>>[phi]=GDN(Img,J,mx,my,theta,sigma,maxit,tol);`
`>> phi= conv2(phi,K_sigma,'same');R=Residual(phi,oldphi)/norm(oldphi);`
`>> if R<tol, break, end >> end; >> figure, imagesc(phi);colormap gray;`




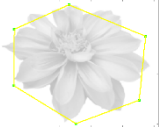





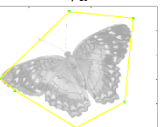
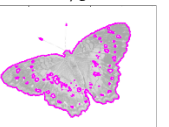

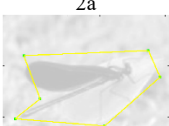
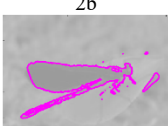
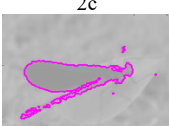

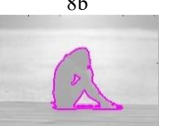

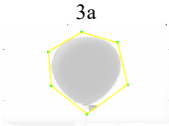
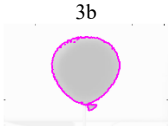
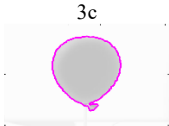
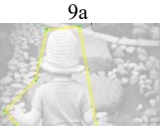
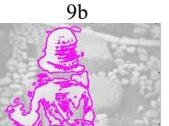
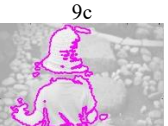
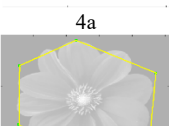
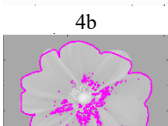


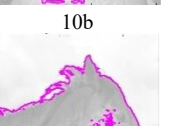
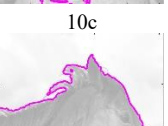
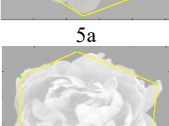
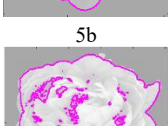

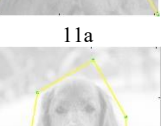
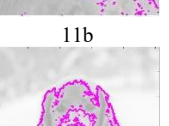
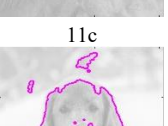
2.4. Performance evaluation

In the final phase, performance accuracy with regard to the model will be assessed utilizing Error, Jaccard and Dice metrics to compare the results. The $Error = 1 - (TP + TN)/(TP + FN + FP + TN)$. Here, true positive (TP) refers to a pixel (or region) that is correctly examined as part of the targeted object. At the same time, the true negative (TN) represents a pixel (or region) that is correctly analyzed as not being part of the targeted object. On the other hand, the false positive (FP) represents a pixel (or region) that is incorrectly labeled as part of the targeted object when it is actually not, while the false negative (FN) denotes a pixel (or region) that is incorrectly labeled as not being part of the targeted object when it actually is. In addition, a low value approaching 0 indicates that the model accurately segments the input images. The formula for Jaccard $= |S_n \cap S_*| / |S_n \cup S_*|$ and Dice $= |S_n \cap S_*| / (|S_n| + |S_*|)$ where S_n is the set of segmented domains of the targeted object and S_* is the true set of the targeted object. The return value of the similarity function is between the range of 0 and 1. Notably, the closer the result value to 1, the higher the level of perfection of the segmentation. The efficiency concerning the suggested GDN model was analyzed by computing the processing time. The experiments were conducted on an AMD Ryzen 7 5700X with Nvidia GeForce 1070, operating at 3.80 GHz and equipped with 32GB of RAM. The processing time was accurately measured utilizing the 'tic' and 'toc' functions in MATLAB R2023a software.

3. RESULTS AND DISCUSSION

Section 3 defines the numerical experiments conducted and the findings obtained. In this study, all real test images were segmented employing the existing GRSS model [12] as well as the proposed GDN model. The parameters tol , $maxit$, and θ are set to 10^{-6} , 100, and 80, respectively, for both models. Meanwhile, the parameters α_1 and α_2 are set in the range of $\alpha_1, \alpha_2 = [0.5, 10]$, and normally $\alpha_1 > \alpha_2$ for images with haze while the parameter σ is set to $\sigma = [10, 200]$. The results of these settings are tabulated in Table 1.

Table 1. The segmentation results

Test Images	GRSS	GDN	Test Images	GRSS	GDN
 1a	 1b	 1c	 7a	 7b	 7c
 2a	 2b	 2c	 8a	 8b	 8c
 3a	 3b	 3c	 9a	 9b	 9c
 4a	 4b	 4c	 10a	 10b	 10c
 5a	 5b	 5c	 11a	 11b	 11c
 6a	 6b	 6c	 12a	 12b	 12c

The first and fourth columns of Table 1 display all the hazy test images that contain objects requiring segmentation. The object designated for segmentation is indicated by green markers and a yellow initial contour. The second and fifth columns of Table 1 demonstrate the results using the GRSS model, while the third and last columns of Table 1 are the results from the GDN model. Visual observation reveals that the GRSS model's segmentation results clearly demonstrate over-segmentation compared to the proposed GDN model. This is due to the fact that the GRSS model cannot clearly define the haze in the images in Table 1 (5b, 6b, 7b, 8b, 11b). According to Ali *et al.* [26], it can be challenging to segment a real image with the presence of haze. The segmentation outcomes from GDN indicate that the input images are more effectively segmented. The main reason for this is that the dehazing process, that is the DehazeNet [27], was added to the GDN model. In particular, the DehazeNet can reduce the haze in the original image [27]. Consequently, the segmentation results of the proposed GDN are better compared to the GRSS model. Additionally, the effectiveness of both models indicated by error, dice, and Jaccard are computed as well to support the results from visual observation. Moreover, the processing time is also recorded to measure efficiency. Table 2 tabulates all the quantitative values.

Table 2. The values of error, dice, Jaccard, and processing time (time)

Test Image	Error		Dice		Jaccard		Time	
	GRSS	GDN	GRSS	GDN	GRSS	GDN	GRSS	GDN
1	0.0430	0.0315	0.8717	0.9100	0.7726	0.8349	7.550	11.930
2	0.0406	0.0395	0.7264	0.7352	0.5703	0.5813	7.760	11.150
3	0.0772	0.0756	0.7399	0.7407	0.5872	0.5881	7.540	11.300
4	0.0093	0.0059	0.9719	0.9824	0.9453	0.9654	7.300	11.770
5	0.0436	0.0153	0.9565	0.9852	0.9166	0.9708	22.600	41.400
6	0.0930	0.0274	0.9157	0.9765	0.8445	0.9541	19.590	34.410
7	0.0730	0.0272	0.9239	0.9729	0.8586	0.9473	19.730	35.060
8	0.0479	0.0279	0.9270	0.9587	0.8640	0.9206	19.200	33.890
9	0.0199	0.0198	0.9101	0.9117	0.8350	0.8377	4.880	6.1200
10	0.1298	0.0778	0.7293	0.8504	0.5739	0.7397	5.760	7.5100
11	0.0437	0.0363	0.9587	0.9663	0.9207	0.9348	19.100	34.170
12	0.1285	0.0742	0.8058	0.8989	0.6748	0.8164	8.800	13.160
Average	0.0625	0.0382	0.8697	0.9074	0.7803	0.8409	12.484	20.989

Based on Table 2, the GDN model consistently achieved the lowest Error value across most datasets for real images. The mean Error value with regard to the GDN model is 0.0382, while the mean error value for the GRSS model is 0.0625. The minimal value of the Error indicates optimal accuracy in image segmentation. The GDN model earned the highest Dice value across almost all the datasets. The DSC value average for the GDN model is 0.9074, surpassing the GRSS model. This result signifies that the GDN model achieved the highest segmentation accuracy in comparison to the existing GRSS model, having an average of 0.8697. At the same time, the GDN model consistently achieved the highest Jaccard value across most of the data. The mean Jaccard value for the GDN model is 0.8409. The GRSS model yields the lowest Jaccard value with an average Jaccard value of 0.7803. The highest value of Jaccard indicates a higher accuracy in image segmentation.

These findings are parallel with the visual observation based on Table 1 made above. Additionally, these results are evidence of the advantages of combining the image dehazing technique with ACM in a new proposed formulation of the GDN model that is capable of producing more precise segmentation in comparison to the original GRSS model. However, incorporating the dehazing technique results in a higher computation cost when formulating the proposed GDN compared to the existing GRSS model. Thus, the average processing time for the GRSS model is the fastest at 12.484 seconds, followed by the GDN model at 20.989 seconds. To conclude, although the proposed GDN model is slower than the GRSS model, the experiments revealed that the GDN model based on the DehazeNet dehazing technique produced the highest accuracy, as demonstrated by the higher average values of Jaccard, as well as Dice values, and the lowest Error value compared to the GRSS model.

4. CONCLUSION

This work reformulates the GRSS model for hazy image segmentation, using the DehazeNet dehazing approach as additional fitting parameters, resulting in a modified variation known as the GRSS with DehazeNet (GDN) model. This research's findings determined that the proposed GDN model generated better image segmentation quality in comparison to the GRSS model, as the dehazing term in the GDN model was capable of reducing the image haze and consequently helped in generating high segmentation accuracy. The outcomes may benefit several applications, including object tracking, driverless (autonomous) cars, and traffic surveillance. The primary limitation of the proposed approach lies in its high processing time, which affects overall efficiency. Consequently, future research may focus on developing faster optimization strategies to solve the model more efficiently. A more comprehensive evaluation across diverse environments and application domains is also necessary to further validate the model's robustness and generalizability. In addition, the model has the potential to be extended to color image segmentation by incorporating alternative dehazing techniques or color space transformations. Although this study concentrated on grayscale images to establish the model's core performance, future work will investigate its adaptation to color images, which could enhance its relevance to real-world scenarios. While this study focused on static image segmentation, the proposed model also shows promise for real-time applications, including video-based segmentation. Future research may explore its implementation in real-time scenarios by integrating optimization techniques aimed at reducing computational latency. Furthermore, evaluating the model on sequential video data would enable assessment of its temporal consistency and segmentation robustness, thereby supporting its practical deployment in fields such as medical imaging, surveillance, and autonomous systems.

ACKNOWLEDGMENTS

The authors extend their sincere gratitude to Universiti Teknologi MARA (UiTM) for supporting this research.

FUNDING INFORMATION

This research received no specific grant from any funding agency in the public, commercial, or not-for-profit sectors.

AUTHOR CONTRIBUTIONS STATEMENT

This journal uses the Contributor Roles Taxonomy (CRediT) to recognize individual author contributions, reduce authorship disputes, and facilitate collaboration.

Name of Author	C	M	So	Va	Fo	I	R	D	O	E	Vi	Su	P	Fu
Firhan Azri Ahmad	✓	✓	✓	✓	✓	✓		✓	✓	✓	✓			
Khairul Anuar														
Jenevy Jone	✓	✓	✓	✓	✓	✓		✓	✓	✓	✓			
Raja Farhatul Aiesya	✓	✓	✓	✓	✓	✓		✓	✓	✓	✓			
Raja Azhar														
Abdul Kadir Jumaat	✓	✓	✓	✓			✓	✓		✓		✓	✓	✓

C : Conceptualization

M : Methodology

So : Software

Va : Validation

Fo : Formal analysis

I : Investigation

R : Resources

D : Data Curation

O : Writing - Original Draft

E : Writing - Review & Editing

Vi : Visualization

Su : Supervision

P : Project administration

Fu : Funding acquisition

CONFLICT OF INTEREST STATEMENT

Authors state no conflict of interest.

DATA AVAILABILITY

The resources underpinning the findings of this study are publicly accessible in references [28]–[32].

REFERENCES

- [1] F. A. Shewajo and K. A. Fante, "Tile-based microscopic image processing for malaria screening using a deep learning approach," *BMC Medical Imaging*, vol. 23, no. 1, pp. 1–14, 2023, doi: 10.1186/s12880-023-00993-9.
- [2] A. M. Anter and L. Abualigah, "Deep federated machine learning-based optimization methods for liver tumor diagnosis: A review," *Archives of Computational Methods in Engineering*, vol. 30, no. 5, pp. 3359–3378, 2023, doi: 10.1007/s11831-023-09901-4.
- [3] S. Srinivasan, P. S. M. Bai, S. K. Mathivanan, V. Muthukumar, J. C. Babu, and L. Vilcekova, "Grade classification of tumors from brain magnetic resonance images using a deep learning technique," *Diagnostics*, vol. 13, no. 6, p. 1153, 2023, doi: 10.3390/diagnostics13061153.
- [4] Z. Q. Habeeb, B. Vuksanovic, and I. Q. Al-Zaydi, "Breast cancer detection using image processing and machine learning," *Journal of Image and Graphics (United Kingdom)*, vol. 11, no. 1, pp. 1–8, 2023, doi: 10.18178/joig.11.1.1-8.
- [5] I. Mishra, K. Aravinda, J. A. Kumar, C. Keerthi, R. Divya Shree, and S. Srikumar, "Medical imaging using signal processing: A comprehensive review," in *Proceedings of the 2nd International Conference on Artificial Intelligence and Smart Energy, ICAIS 2022*, 2022, pp. 623–630. doi: 10.1109/ICAIS53314.2022.9742778.
- [6] M. I. Yeşil and S. Göncü, "Recognition of Hereford and Simmental cattle breeds via computer vision," *Iranian Journal of Applied Animal Science*, vol. 13, no. 1, pp. 21–32, 2023.
- [7] J. Fang, H. Liu, L. Zhang, J. Liu, and H. Liu, "Region-edge-based active contours driven by hybrid and local fuzzy region-based energy for image segmentation," *Information Sciences*, vol. 546, pp. 397–419, 2021, doi: 10.1016/j.ins.2020.08.078.
- [8] R. Yousef *et al.*, "U-Net-based models towards optimal MR brain image segmentation," *Diagnostics*, vol. 13, no. 9, p. 1624, 2023, doi: 10.3390/diagnostics13091624.
- [9] K. Chen, "Introduction to variational image-processing models and applications," *International Journal of Computer Mathematics*, vol. 90, no. 1, pp. 1–8, 2013, doi: 10.1080/00207160.2012.757073.
- [10] G.-L. Zhu, X.-G. Lv, F. Li, and X.-M. Sun, "Nonconvex variational approach for simultaneously recovering cartoon and texture images," *Journal of Electronic Imaging*, vol. 31, no. 04, p. 43021, 2022, doi: 10.1117/1.jei.31.4.043021.
- [11] X. Liu, G. Liu, Y. Wang, G. Li, R. Zhang, and W. Peng, "A variational level set image segmentation method via fractional differentiation," *Fractal and Fractional*, vol. 6, no. 9, p. 462, 2022, doi: 10.3390/fractalfract6090462.
- [12] T. C. Saibin and A. K. Jumaat, "Variational selective segmentation model for intensity inhomogeneous image," *Indonesian Journal of Electrical Engineering and Computer Science (IJECS)*, vol. 29, no. 1, pp. 277–285, 2023, doi: 10.11591/ijeecs.v29i1.p277-285





- 10.11591/ijeeecs.v29.i1.pp277-285.
- [13] J. Gu, Z. Fang, Y. Gao, and F. Tian, "Segmentation of coronary arteries images using global feature embedded network with active contour loss," *Computerized Medical Imaging and Graphics*, vol. 86, p. 101799, 2020, doi: 10.1016/j.compmedimag.2020.101799.
 - [14] Y. Yang, W. Jia, and B. Wu, "Simultaneous segmentation and correction model for color medical and natural images with intensity inhomogeneity," *Visual Computer*, vol. 36, no. 4, pp. 717–731, 2020, doi: 10.1007/s00371-019-01651-4.
 - [15] E. Iqbal, A. Niaz, A. A. Memon, U. Asim, and K. N. Choi, "Saliency driven region-edge-based top down level set evolution reveals the asynchronous focus in image segmentation," *IEEE Access*, vol. 8, pp. 208978–208991, 2020, doi: 10.1109/ACCESS.2020.3038945.
 - [16] X.-H. Zhi and H.-B. Shen, "Saliency driven region-edge-based top down level set evolution reveals the asynchronous focus in image segmentation," *Pattern Recognition*, vol. 80, pp. 241–255, Aug. 2018, doi: 10.1016/j.patcog.2018.03.010.
 - [17] W. Zhao, W. Wang, X. Feng, and Y. Han, "A new variational method for selective segmentation of medical images," *Signal Processing*, vol. 190, p. 108292, 2022, doi: 10.1016/j.sigpro.2021.108292.
 - [18] N. A. S. M. Ghani and A. K. Jumaat, "Selective segmentation model for vector-valued images," *Journal of Information and Communication Technology*, vol. 21, no. 2, pp. 149–173, 2022, doi: 10.32890/jict2022.21.2.1.
 - [19] N. A. S. M. Ghani, A. K. Jumaat, R. Mahmud, M. A. Maasar, F. A. Zulkifle, and A. M. Jasin, "Breast abnormality boundary extraction in mammography image using variational level set and self-organizing map (SOM)," *Mathematics*, vol. 11, no. 4, p. 976, 2023, doi: 10.3390/math11040976.
 - [20] S. S. Yasiran *et al.*, "Comparison between GVF snake and ED snake in segmenting microcalcifications," in *ICCAIE 2011 - 2011 IEEE Conference on Computer Applications and Industrial Electronics*, Dec. 2011, pp. 597–601. doi: 10.1109/ICCAIE.2011.6162204.
 - [21] N. A. K. Zaman, W. E. Z. W. A. Rahman, A. K. Jumaat, and S. S. Yasiran, "Classification of breast abnormalities using artificial neural network," in *AIP Conference Proceedings*, May 2015, vol. 1660, no. 1, p. 50038. doi: 10.1063/1.4915671.
 - [22] N. Badshah and K. Chen, "Image selective segmentation under geometrical constraints using an active contour approach," *Communications in Computational Physics*, vol. 7, no. 4, pp. 759–778, 2010, doi: 10.4208/cicp.2009.09.026.
 - [23] L. Rada and K. Chen, "Improved selective segmentation model using one level-set," *Journal of Algorithms and Computational Technology*, vol. 7, no. 4, pp. 509–540, 2013, doi: 10.1260/1748-3018.7.4.509.
 - [24] J. Spencer and K. Chen, "A convex and selective variational model for image segmentation," *Communications in Mathematical Sciences*, vol. 13, no. 6, pp. 1453–1472, 2015, doi: 10.4310/CMS.2015.v13.n6.a5.
 - [25] A. K. Jumaat and K. Chen, "A reformulated convex and selective variational image segmentation model and its fast multilevel algorithm," *Numerical Mathematics*, vol. 12, no. 2, pp. 403–437, Jun. 2019, doi: 10.4208/nmtma.OA-2017-0143.
 - [26] H. Ali, A. Sher, M. Saeed, and L. Rada, "Active contour image segmentation model with de-hazing constraints," *IET Image Processing*, vol. 14, no. 5, pp. 921–928, 2020, doi: 10.1049/iet-ipr.2018.5987.
 - [27] B. Cai, X. Xu, K. Jia, C. Qing, and D. Tao, "DehazeNet: An end-to-end system for single image haze removal," *IEEE Transactions on Image Processing*, vol. 25, no. 11, pp. 5187–5198, Nov. 2016, doi: 10.1109/TIP.2016.2598681.
 - [28] V. T. Pham, "How to use Detectron2," *GitHub*. <https://github.com/facebookresearch/detectron2/issues/795> (accessed Feb. 05, 2024).
 - [29] J. Li, J. Zhang, and D. Tao, "Deep automatic natural image matting," *CoRR*, vol. abs/2107.0, 2021.
 - [30] Y. Qiao *et al.*, "Attention-guided hierarchical structure aggregation for image matting," in *Proceedings of the IEEE Computer Society Conference on Computer Vision and Pattern Recognition*, 2020, pp. 13673–13682. doi: 10.1109/CVPR42600.2020.01369.
 - [31] H. Li, J. Cai, T. N. A. Nguyen, and J. Zheng, "A benchmark for semantic image segmentation," in *Proceedings - IEEE International Conference on Multimedia and Expo*, 2013, pp. 1–6. doi: 10.1109/ICME.2013.6607512.
 - [32] M. Y. Chen *et al.*, "Automatic Chinese food identification and quantity estimation," in *SIGGRAPH Asia 2012 Technical Briefs, SA 2012*, 2012. doi: 10.1145/2407746.2407775.

BIOGRAPHIES OF AUTHORS






Firhan Azri Ahmad Khairul Anuar     is a student of the B.Sc. degree in Mathematics from Universiti Teknologi MARA (UiTM) Shah Alam. His research interests revolve around mathematical modeling and image processing. He can be contacted at 2023104939@student.uitm.edu.my.






Jenevy Jone     obtained her B.Sc. degree in Mathematics from Universiti Teknologi MARA (UiTM) Shah Alam. She is currently working as a finance risk cost control assistant at Shangri-La Rasa Ria, Kota Kinabalu. Her research interests revolve around mathematical modeling and image processing. She can be contacted at jenevyjone@gmail.com.



Raja Farhatul Aiesya Raja Azhar    obtained her B.Sc. degree in Mathematics from Universiti Teknologi MARA (UiTM) Shah Alam and is currently pursuing a Master of Computer Science (Computational Intelligence) at Universiti Malaysia Sabah. Her studies focus on computational intelligence techniques, including nature-inspired computing, artificial neural networks, and multi-objective optimization. Her research interests revolve around mathematical modeling and image processing. She can be contacted at aiesya77@yahoo.com.



Abdul Kadir Jumaat    obtained the B.Sc. and M.Sc. degrees in Mathematics from Universiti Teknologi MARA (UiTM) Shah Alam, Malaysia, and the University of Liverpool in the United Kingdom awarded him a Ph.D. degree, particularly in applied mathematics (mathematical imaging methods). Presently, he holds the position of senior lecturer at the School of Mathematical Sciences, Faculty of Computer and Mathematical Sciences, and a research fellow at the Institute for Big Data Analytics and Artificial Intelligence (IBDAAI) in UiTM Shah Alam, Malaysia. His research interests encompass various fields such as image/signal processing, artificial intelligence, computer vision, biometrics, medical image and analysis, and pattern recognition. His email address is abdulkadir@tmsk.uitm.edu.my.